GEOPHYSICAL RESEARCH LETTERS, VOL. 28, NO. 11, PAGES 2285-2288, JUNE 1, 2001

Fault geometry and slip distribution of the 1999 Chi-Chi, Taiwan earthquake imaged from inversion of GPS data

Kaj M. Johnson,[1] Ya-Ju Hsu,[2] Paul Segall,[1] and Shui-Beih Yu[3]

Abstract. GPS measurements of coseismic displacements from the 1999, Chi-Chi, Taiwan earthquake are modeled using elastic dislocation theory. We find that a single fault plane cannot fit the data, but rather a curved fault surface consisting of multiple segments dipping 20-25° best fits the observations. The model fault exhibits reverse and left-lateral slip on a 75 km long N-S trending segment and reverse and right-lateral slip on a 25 km E-W trending segment at the northern end of the rupture. The 21° dipping E-W segment is inconsistent with previous interpretations of high angle tear faulting.

1. Introduction

The 21 September, 1999 Chi-Chi, Taiwan earthquake (Mw = 7.5) occurred along the previously recognized north-south trending Chelungpu fault, generating over 100 km of surface rupture extending from Chushan to Shuangchi (Figure 1) [Kao and Chen, 2000]. The main shock initiated near the town of Chi-Chi at 10 km depth and propagated north towards the town of Fengyuan [Ma et al., 2000] where the maximum surface offset of 11 m occurred. Coseismic displacements of the Chi-chi earthquake were determined by Yu et al. [2000] using the Taiwan global positioning system (GPS) network consisting of more than 150 campaign stations and 45 continuously recording permanent stations. Yu et al. [2000] show that the horizontal surface displacements increase from 1 m at the southern end of the fault trace to 9 m at the northern end (Figure 1). The vertical offsets were largest near the fault trace, where the hanging wall was uplifted as much as 4.4 meters, and decrease rapidly toward the east. The stations on the footwall side show smaller horizontal displacements ranging from 0.2 to 1.5 m and subsidence of 0.02-0.32 m.

Kao and Chen [2000] combined hypocenter and fault plane solutions of more than 40 aftershocks to show that the earthquake occurred on a 20-30° east dipping fault. Inversion of teleseismic data by Ma et al. [2000] indicates a patch of large slip (up to 12 m) near the ground surface north of Fengyuan at the bend in the fault trace. The Harvard CMT mechanism has one plane striking 37 and dipping 25° to the east with a scalar moment 3.4×10^{20} N-m. The NEIC mechanism strikes more northerly (357°), with similar dip (29°), but smaller moment (2.4×10^{20} N-m).

[1]Geophysics Department, Stanford University, Stanford, CA.
[2]Institution of Geophysics, National Central University, Chungli, Taiwan.
[3]Institute of Earth Sciences, Academia Sinica, Taipei, Taiwan.

Paper number 2000GL012761.
0094-8276/01/2000GL012761$05.00

Surface deformation along the N-S trending Chushan-Fengyuan section of the fault (Figure 1) is consistent with reverse and left-lateral slip on a shallow (∼30°) thrust fault. However, interpretation of subsurface fault geometry is not so clear along the Fengyuan-Shuangchi section where the surface rupture is marked by discontinuous traces of reverse and normal faults, some of which display right-lateral offsets [Huang et al., 1999]. Strike slip aftershocks in this area suggest high-angle tear faulting [Kao and Chen, 2000].

In this study we estimate the subsurface fault geometry and coseismic slip distribution of the Chi-Chi earthquake using the GPS measurements of Yu et al. [2000], assuming that the fault can be approximated with dislocations in a homogeneous elastic half-space.

2. Data Collection and Processing

Annual surveys at 71 stations and initial epoch surveys at 40 stations were conducted in the eight-year period leading up to the Chi-chi earthquake, from 1992 to 1999 [Yu et al., 2000]. The 71 stations surveyed annually were resurveyed at least once within 15 days following the main shock. The other 40 stations were resurveyed in December, 3 months following the earthquake. All data were processed with Bernese software v. 4.0. The coseismic displacements of the campaign stations are estimated with respect to Kinmen (about 257 km from the epicenter) which didn't show significant coseismic movement. The coseismic displacements of the permanent stations are determined from daily solutions, fixing the coordinates and velocities of 12 global IGS stations to their I.T.R.F. 97 values. Yu et al. [2000] corrected the data for pre-seismic secular motions by fitting a first order trend surface to the velocity of 24 stations, which were collected from 1992 to 1999. Corrections for post-seismic displacements at the stations surveyed in December were interpolated from the nearby continuous stations or campaign stations with several post-seismic measurements. Details of the data collection and processing are given in Yu et al. [2000].

3. Analysis of Fault Geometry and Slip Distribution

3.1. One-fault model

We begin with the simplest model and assume the fault can be approximated with a single dislocation with variable slip extending the 75 km length of the fault trace from Chushan to Fengyuan (Figure 1). The analysis is a two-step process; we initially optimize the dip and down-dip width of a uniform slip dislocation and subsequently fix this optimal fault geometry to solve for the slip distribution.

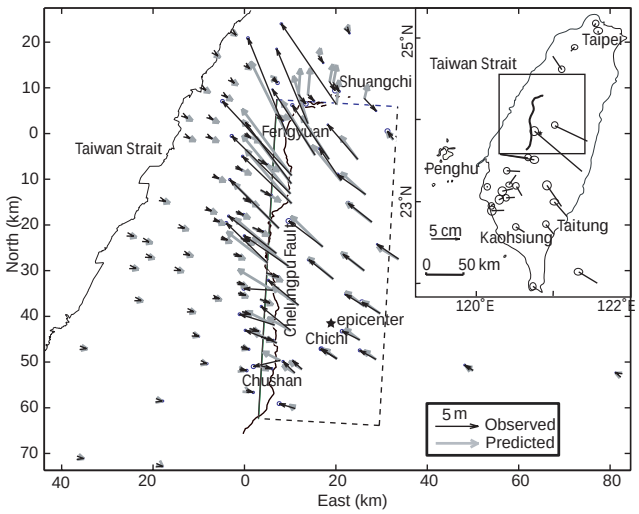

Figure 1. One-fault model and location of Chelungpu fault and 128 GPS stations used in this study. Horizontal coseismic displacement vectors show large displacements near the fault trace that rapidly decrease away from the fault. Error ellipses indicate 95% confidence intervals. Rectangle marks the surface projection of the model fault plane. Note the one-fault model does not fit the data at the northern end. Inset shows location of Chelungpu fault in western Taiwan and coseismic displacements at far-field stations.

Numerous authors have presented methods for estimating source geometry [e.g. Cervelli et al. 2001] and slip distribution [e.g. Hudnut et al., 1993] given coseismic displacements. The measured GPS displacements, d, are related to the slip, s, by

$$d = \mathbf{G}s + \varepsilon \tag{1}$$

in which $\mathbf{G}$ is a function of the dislocation model parameters (strike, dip, length, width, depth, horizontal position) and is computed assuming a uniform, isotropic elastic half-space, and ε is measurement error. For the one-fault model, the strike, length, depth and horizontal position are selected to correspond with the trace of the mapped surface rupture. The remaining parameters (dip, width, slip) are determined using a quasi-Newton nonlinear optimization algorithm. We find the optimal dip and width to be 28° and 30 km respectively.

The slip distribution is approximated by discretizing the fault plane into rectangular patches of uniform dislocation and simultaneously minimizing the data misfit and the model roughness by minimizing the functional

$$F(s,\gamma) = ||\mathbf{G}s - d||^2 + \gamma^{-2}||\bigtriangledown^2 s||^2 \tag{2}$$

subject to the constraint that $s_i \geq 0$ for all patches, i. The smoothing operator $\bigtriangledown^2$ is the finite difference approximation of the Laplacian operator, and γ serves as a measure of the roughness of the slip distribution [e.g. Harris and Segall, 1987]. The first term on the right side of (2) measures the model misfit while the second term measures the roughness. The parameter γ therefore determines the relative weight placed on fitting the data versus smoothing the slip distribution.

The smoothing parameter, γ, in (2) can be determined objectively with the statistical method of cross-validation [Mathews and Segall, 1993]. We invert for variable slip on the fault plane with $\gamma = 0.015$, as determined by cross-validation. We find (Figure 1) that predicted displacement vectors at the northern end of the fault are directed nearly 180° to the measured displacements. This is true regardless of choice of γ, indicating that a single fault cannot fit the observations.

3.2. Three-fault model

To improve the model at the northern end of the rupture, two additional segments are included (Figure 2). The three fault model includes a 70 km long N3E segment, an 8 km segment trending N35E at the bend where the surface rupture curves to the east, and a 25 km segment trending N88E to the east of Fengyuan.

We assigned a width of 30 km to the three fault planes and simultaneously estimated the dips and slip distribution. As before, the strike, length, and position of the three fault planes were selected to correspond with the mapped surface

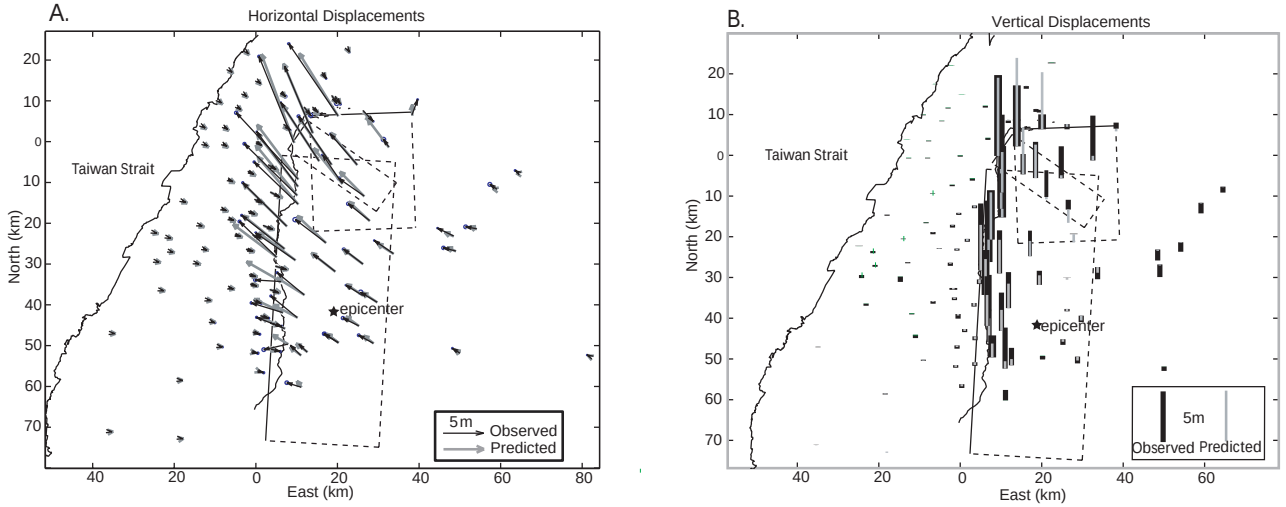

Figure 2. Displacements for the three-fault model. Rectangles mark the surface projections of the model fault planes. A. Horizontal displacements. B. Vertical displacements.

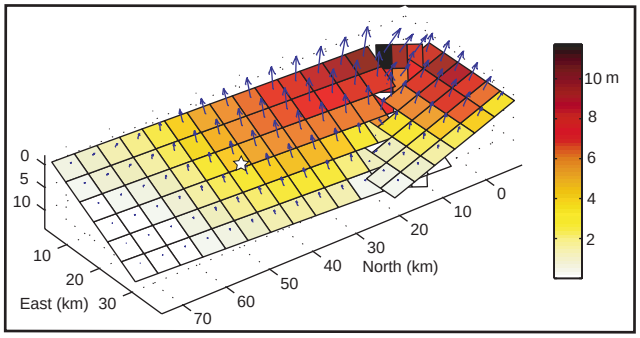

Figure 3. Slip distribution for three-fault model. Vectors indicate rake. Maximum slip of 11 m occurs near ground surface at the bend in the fault. Left-lateral and thrust components of slip on N3E and N35E segments. Right-lateral and thrust components of slip on N88E segment.

ruptures. To solve for the dips and slip distribution, we cycled through 18 dip angles, in the range 0-50°, for each fault plane and inverted for the slip distribution across the three planes for all 18^3 models. The weighted residual sum of squares (WRSS) is minimized for dips of 23° (N3E fault), 23° (N35E fault), and 21° (N88E fault). Finally, we again fix this fault geometry and determine the optimal smoothing parameter by cross validation ($\gamma = 0.025$). This produces the slip distribution in Figure 3. We see that including the fault segments at the northern end greatly improves the fit to the data (Figure 2). The WRSS is reduced by a factor of five.

4. Discussion

The gross trend in net slip at the ground surface agrees well with field measurements (Figure 4A). Both the model and field measurements indicate an increase in net slip from less than three meters at the southern end of the fault to the maximum value of about 11 m at the northern end where the fault trace curves to the east. The slip over the entire fault plane is qualitatively similar to the slip distribution estimated by teleseismic inversion [Ma et al., 2000]. In both models there is a patch of large slip, with maximum 11 m, concentrated at the northern bend in the fault, extending about 10 km (in the direction of the dip) from the ground surface. Both models show only one or two meters of net slip at the hypocenter.

The fault geometry inferred from our model is not entirely consistent with the fault geometry estimated from seismic data. The 23°dipping thrust along the long N3E trending section of the fault is consistent with fault plane solutions presented by Kao and Chen [2000]. However, Kao and Chen report high angle strike slip faulting at depths of 12-33 km at both ends of the fault which is inconsistent with the shallow dipping E-W fault in our model. Furthermore, we have found that a steeply dipping fault plane along the E-W fault segment cannot fit the data, regardless of the slip distribution. The WRSS with a vertical E-W fault is nearly five times larger than the WRSS with a 21° dipping E-W thrust fault.

The moment in the geodetic inversion is 2.8×10^{20} N-m, which falls between the moments determined by NEIC (2.4×10^{20} N-m) and Harvard (3.4×10^{20} N-m). The best fitting double couple representation (Figure 4B) is in good agreement with the Harvard CMT solution. The fact that the strike of the CMT solution does not coincide with the N-S surface rupture suggests that slip on the E-W segment occured within about 200 seconds of the earthquake's centroid time, based on the period of the surface waves used in the inversion.

The three fault model explains the gross kinematics of the coseismic displacements and 98% of the variance in the data. However, the displacement vectors do not fit the measurements to within the uncertainties. The weighted root mean square misfit [Segall and Harris, 1986] is 0.19 m, well above the measurement uncertainty. Thirteen sites disagree by more than one meter in the vertical and five sites disagree by more than a meter in the horizontal. Furthermore, the residuals are spatially coherent. The model over-predicts the footwall displacements at 31 of 36 (86%) sites west of the fault trace and under-predicts the vertical displacements (in magnitude) at 101 of the total 128 sites (79%). The large and spatially coherent residuals may be attributed to elastic heterogeneity, topography, as well as inelastic deformation, all of which are ignored in this simplified model. For example, because the Chelungpu fault surfaces between the low lying coastal plain and the high Western Foothills, topography may influence the surface displacements. Furthermore, in addition to vertical variation in elastic moduli, Cheng [2000] shows lateral heterogeneity across the Chelungpu fault as a result of older, less compliant rock thrusted over younger sediments. Further research will be directed toward the study of heterogeneity and topography effects.

5. Conclusions

Inversion of coseismic GPS data using elastic dislocation theory provides an estimate of the subsurface fault geometry and slip distribution of the Chi-Chi earthquake. We have found that a single fault plane cannot fit the data. A model in which the fault dips 20-25° and curves north of Fengyuan and follows the trend of the E-W ground ruptures greatly improves the fit to the GPS data. The model contains reverse slip everywhere on the fault, but the Chushan-Fengyuan section has a large left-lateral component of slip while the Fengyuan-Shuangchi section has a large righ-lateral component. The gross slip distribution in our model is consistent with teleseismic results. Both methods suggest the largest slip occurs near the ground surface at the northern bend in the fault, coincident with largest displacements and slips measured at the ground surface. However, the model is inconsistent with focal mechanisms that show high angle strike-slip faulting at both ends of the fault.

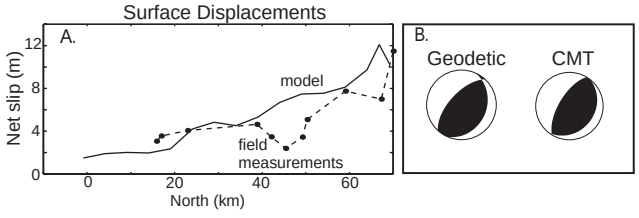

Figure 4. A. Comparison of the estimated fault slip at the ground surface with field measurements. B. Best fitting double couple representation of the geodetic moment tensor compared to the Harvard CMT solution.

References

Cervelli, P., Murray, M.H., Segall, P., Aoki, Y., and Kato, T., Estimating source parameters from deformation data, with an application to the March 1997 earthquake swarm off the Izu Peninsula, Japan, in press, *J. Geophys. Res.,* 2001.

Arnadottir, T., and P. Segall, P., The 1989 Loma Prieta earthquake imaged from inversion of geodetic data, *J. Geophys. Res., 99,* 21835-21855, 1994.

Cheng, W. B., Three-dimensional crustal structure around the source area of the 1999 Chi-Chi earthquake in Taiwan and its relation to the aftershock locations, i*TAO, 11,* 643-660, 2000.

Harris, R., and P. Segall, Detection of a locked zone at depth on the Parkfield, California, segment of the San Andreas fault, *J. Geophys. Res., 92,* 7945-7962, 1987.

Huang, C.Y., C. W. Lin, W. S. Chen, Y. G. Chen, S. B. Yu, I. P. Chia, M. D. Lu, C. S. Hou, and Y. S. Wang, Seismic geology of the Chi-Chi earthquake, paper presented at International Workshop on Chi-Chi, Taiwan Earthquake of Sept 21, 1999, 1999.

Hudnut, K.W., Y. Bock, M. Cline, P. Fang, Y. Feng, J. Freymueller, X. Ge, W.K. Gross, D. Jackson, M. Kim, N.E. King, J. Langbein, S.C. Larsen, M. Lisowski, Z.K. Shen, J. Svarc, and J. Zhang, Coseismic displacements of the 1992 Landers earthquake sequence, *Bull. Seismol. Soc. Am.,* it 84, 3, 625-645, 1993.

Kao, H., and W. P. Chen, The Chi-Chi earthquake sequence: active, out-of-sequence thrust faulting in Taiwan, *Science, 288,* 2346-2349, 2000.

Ma, K.F., Song, T.R, Lee, S.J., and Wu, H.I., Spatial slip distribution of the September 20, 1999, Chi-Chi, Taiwan, earthquake (Mw7.6) - Inverted from teleseismic data, *Geophys. Res. Lett., 27, 20,* 3417-3420, 2000.

Mathews, M., and P. Segall, Statistical inversion of crustal deformation data and estimation of the depth distribution of slip in the 1906 earthquake, *J. Geophys. Res., 98,* 12153-12163, 1993.

Segall, P., and R. Harris, Slip deficit on the San Andreas fault at Parkfield, California, as revealed by inversion of geodetic data, *Science, 233,* 1409-1413, 1986.

Yu, S.B., L.C. Kuo, Y.J. Hsu, H.H. Su, C.C. Liu, C.S. Huo, J.F. Lee, T.C., Lai, C.L., Liu, T.F. Tseng, C.S. Tsai, and T.C. Shin, Preseismic deformation and coseismic displacements associated with the 1999 Chi-Chi, Taiwan earthquake, submitted, *Bull. Seismol. Soc. Am.*

K. M. Johnson, and P. Segall, Geophysics Department, Stanford University, Stanford, CA 94305. (e-mail: kaj@pangea.stanford.edu, segall@pangea.stanford.edu)

Y. J. Hsu, Institution of Geophysics, National Central University, Chung-li, Taiwan, ROC. (e-mail: yaru@earth.sinica.edu.tw)

S. B. Yu, Institute of Earth Sciences, Academia Sinica, P.O. Box 1-55, Nankang, Taipei, Taiwan, R.O.C.

(Received December 12, 2000; accepted January 28, 2001.)